energies

MDPI

Article

Certainty-Equivalence-Based Sensorless Robust Sliding Mode Control for Maximum Power Extraction of an Uncertain Photovoltaic System

Zaheer Alam [1], Qudrat Khan[2], Laiq Khan [3], Safeer Ullah [3,*], Syed Abdul Mannan Kirmani [2] and Abdullah A. Algethami [4]

[1] Electrical Engineering Department, COMSATS University Islamabad, Abbottabad 22060, Pakistan; zaheerepe068@gmail.com
[2] Centre for Advanced Studies in Telecommunications (CAST), Islamabad Campus, COMSATS University Islamabad, Islamabad 45550, Pakistan; qudratullah@comsats.edu.pk (Q.K.); abdul.mannan@comsats.edu.pk (S.A.M.K.)
[3] Department of Electrical and Computer Engineering, COMSATS University Islamabad, Islamabad 45550, Pakistan; laiq@cuiatd.edu.pk
[4] Department of Engineering, Taif University, Taif 11099, Saudi Arabia; a_Algethami@tu.edu.sa
* Correspondence: safeer_iiui@yahoo.com; Tel.: +92-313-9067608

Abstract: Photovoltaic (PV) arrays and their electronic converters are subject to various environmental disturbances and component-related faults that affect their normal operations and result in a considerable energy loss. Therefore, it is ever demanding to design such closed-loop operating algorithms that tolerate faults, present acceptable performance, and avoid wear and tear in the systems. In this work, the core objective is to extract maximum power from a PV array subject to environmental disturbances and plant uncertainties. The system is considered under input channel uncertainties (i.e., faults) along with variable resistive load and charging stations. A neuro-fuzzy network (NFN)-based reference voltage is generated to extract maximum power while considering variable temperature and irradiance as inputs. Furthermore, the estimated reference is tracked by the actual PV voltage under two types of controllers: certainty-equivalence-based robust sliding mode (CERSMC) and certainty-equivalence-based robust integral sliding mode (CERISMC). These strategies benefit from improving the robustness against faults (disturbances). The proposed methods use the inductor current, which is recovered via the velocity observer and the flatness property of nonlinear systems. The system's stability is proven in the form of very appealing theorems. These claims are validated by the simulation results, which are carried out in a MATLAB environment.

Keywords: arbitrary order sliding mode control; closed-loop stability; feed forward neural network; high gain differentiator; maximum power extraction; photovoltaic system

Citation: Alam, Z.; Khan, Q.; Khan, L.; Ullah, S.; Kirmani, S.A.M.; Algethami, A.A. Certainty-Equivalence-Based Sensorless Robust Sliding Mode Control for Maximum Power Extraction of an Uncertain Photovoltaic System. *Energies* **2022**, *15*, 2029. https://doi.org/10.3390/en15062029

Academic Editor: Alberto Dolara

Received: 7 January 2022
Accepted: 3 March 2022
Published: 10 March 2022

1. Introduction

The ever increasing demand for electrical energy is a prime issue across the globe because of continued reduction in fossil fuels, emission of greenhouse gases, and pollution problems. To overcome these issues, the only solution is the consideration of renewable energy sources. Renewable energy sources are available in different types, e.g., hydropower, geothermal, solar, wind, and biomass. In the current era, the under-study system is one of the most economical and sustainable renewable energy sources [1,2]. Solar energy is more abundant, most prominent, inexhaustible, and clean than the non-renewable energy sources. PV is the most exploited renewable energy source, alongside hydro and wind power, in terms of deployment speed, and it is considered a very promising source of future electrical power generation due to the abundance of sunlight over a large area of the earth's surface, allowing for a variety of PV system applications [3,4]. It also provides ongoing cost reduction over time, a reliable system, rapid technical growth, maintenance-free operation,

and pollution-free operation [5]. Solar energy has become the prime area of active research due to the aforementioned features and characteristics.

Generally, PV systems are categorized into grid-connected, standalone, and hybrid systems. The standalone PV system is the best to use for areas far away from utility grids. These types of systems can generate power ranges from 1 to 100 kW. Although the PV system has attained more attention in the last few decades, one may face specific difficulties while installing these units on a large scale for power generation, such as the cost may increase while its efficiency may not. Therefore, currently, numerous methodologies have been proposed for the solution of these drawbacks of PV systems [6].

Generally, the PV unit provides maximum power to load at maximum power point (MPP) under rapidly changing environmental conditions. At these MPP, the overall PV unit operates with full capacity and maximum efficiency and supplies maximum power where required. Hence, to follow the MPP, a vast number of MPP algorithms are constructed, which are named as Incremental Conductance (IC) [7], Perturb and Observe (P & O) [8], Fuzzy Logic Algorithm (FLA), and Artificial Neural Networks (ANN) [9]. However, to overcome the shortcomings of conventional MPPT algorithms, several studies have highlighted the benefits of using a multi-string topology with distributed dc-dc converters based on global maximum power point tracking (GMPPT) algorithms [10,11]. In order to locate the GMPPT, innovative techniques based on artificial neural networks [12], fuzzy logic [13], dividing rectangle search control [14], and sequential extremum searching control [15] have been successfully employed. In recent years, bioinspired optimization approaches, such as particle swarm optimization [16], ant colony optimization [17], and artificial bee colony [18], have also been used for MPPT from the PV system.

PV-based power generation has been amplified in recent years due to its environmentally friendly nature. However, such wide-scale dissemination of solar panels has never led to performance monitoring and profitability in the presence of the disturbances [19]. The reduction in output power of PV panels is caused either by a fault in the components, such as capacitors, inductors of the converter, or switches, or by some unmodeled plant dynamics. Consequently, these are the components that possibly affect the working of power converters because, very often, these are the most exposed components to high electrical, thermal, and mechanical stress [20]. These stresses cause the failure of the switches, which are further subdivided into open and short-circuit faults (or failures) [21]. A fault in the DC-DC converters will directly affect the performance of the PV system and can cause its complete failure while it is connected to PV array [22]. The power converter failures caused by semiconductor faults are considered to be 21% of total power converter failures [23,24]. The authors of [25] state that the failure of semiconductors and the soldering joints in these converter systems result in around 34% of power system failures. Hence, it is important to reduce these failure rates and avoid the stoppages of a PV system. For this purpose, a robust, precise, and accurate fault-diagnosis and fault-tolerance scheme's development is required to ensure continuous power provision from the PV systems.

In the existing literature, several strategies are proposed for the fault diagnosis of the PV system. Fault diagnosis contains two main approaches. The first one is based on material redundancy, where sensor faults are diagnosed through a comparison between the delivered information from two or more sensors. This is a straightforward and effective process; however, it has several problems, such as large space requirements, extra weight, and high cost. The second fault-diagnosis approach is based on analytical redundancy, which depends on the available sensor information, PV system dynamics, and PV system modeling [26]. In [27], several fault-diagnosis techniques for PV cell has been proposed. Although these techniques diagnose faults, they require extra equipment, such as signal generators for fault diagnosis. In [28], the author presented a review of fault-diagnosis techniques on the DC side of PV arrays; some of the techniques only take into account fault diagnosis, and some both diagnose and classify.

A strategy named as fast detection method (FDM) is proposed in [29], where they have focused on the shape of the inductor current to diagnose the faults and based on which a

fault-tolerant operation is conducted for the PV system's boost converter by employing the fault-diagnosis and reconfiguration strategies on a single field-programmable gate array target. This way, both the open and short circuit faults can be detected, identified, and handled in actuality. Such kinds of schemes have been employed in [30] to a three-level boost converter (in a PV power system) while making use of batteries as storage devices. They proposed a reconfiguration strategy of the PV cells with other cells to bypass the affected one.

Furthermore, variable structure-based designed sliding mode control laws are utilized to treat the matched uncertainties. The conventional sliding mode laws show robustness in sliding mode because of the in-variance property [31–34]; however, these methodologies have not yet invoked the differentiation among the structured and unstructured uncertainties. The only way to cope with uncertain scenarios is to use high gains of the control, but high gains cause substantial chattering [35]. To provide a solution for the chattering phenomena, the certainty equivalence principle (CEP)-based control input was designed for the system in a closed loop that can be capable enough to tolerate the adverse influences of the uncertainties [36]. In the context of CEP, very appealing adaptive laws, based on a super-twisting algorithm (STA), are presented in [36,37] to cope with the family-matched uncertainties. The devised control technique uses an estimator for the uncertainties and, consequently, a big part of the unknown dynamics are made available, which results in low bounds of the uncertainties, and hence the control gains become smaller than the high bound uncertainties. This approach is named a certainty equivalence-based super-twisting algorithm (CESTA). The uncertainties, which are subdivided into unstructured uncertainties, are estimated (or compensated for) by the conventional control part of the CEP, whereas the Lyapunov-function-based adaptation law obtained in [38,39] is used to suppress the unstructured uncertainty (or nullifies the unstructured tension in case of matched uncertainties).

In this paper, the concept of certainty equivalence principle is utilized to design new control approaches (i.e., certainty-equivalence-based robust sliding mode and certainty-equivalence-based robust integral sliding mode) to overcome the excessive chattering problem during faults while extracting the maximum power from a PV array which is accompanied by a buck-boost converter (BBC) The under-study system is considered with a variable resistive load and charging station. A reference voltage is generated via the neuro-fuzzy network. Secondly, the missing states are recovered using a velocity observer and the flatness property of nonlinear systems. Finally, the proposed schemes (CERSMC and CERISMC) are designed to track the reference voltage. The stability of these controllers is comprehensively presented in theorems. All claims are verified in MATLAB/Simulink environment by comparing the simulation results of proposed techniques with STA and ISMC of the existing literature. It is important to note that no such kind of uncertainty-tolerant controller is proposed while dealing with PV systems. In other words, the proposed work, i.e., CERSMC and CERISMC, are novel in their employment to the PV systems.

The rest of the manuscript understudy is organized as follows: the equivalent circuit modeling of PV cell and buck-boost converter of a standalone PV system are presented in Sections 2 and 3 consecutively. Section 4 offers the proposed uncertainty-tolerant MPPT control design, neuro-fuzzy-algorithm-based reference voltage generation for tracking purposes to accomplish the objective of MPPT, the velocity observer for estimation of missing information, the proposed controllers based on CEP, and the stability analysis to prove the stability of zero dynamics of the system. Section 5 contains simulation results and discussion. Some concluding remarks of the proposed research work along future directions are presented in the last section.

2. Equivalent Circuit Modeling of PV Cell

The equivalent circuit models in the technology of PV systems are of prime importance. It presents the overall current-voltage (IV) characteristics curve as a continuous function for a given set of operating conditions. The single diode model, one of the equivalent circuit

models, is equipped via the physical principles [40]. Its most appealing circuit for a single solar cell is displayed in the forthcoming Figure 1.

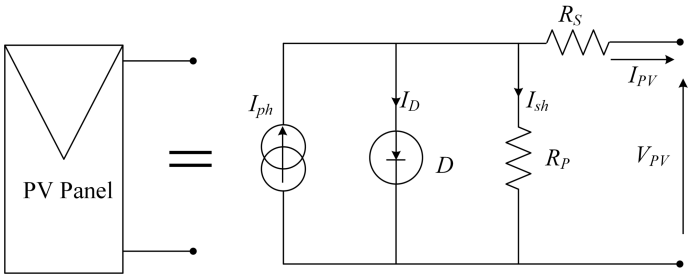

Figure 1. Single-diode model of PV cell

To determine the output PV cell current, I_{pv}, the Kirchoff's current law gives

$$I_{pv} = I_{ph} - I_D - I_{sh} \tag{1}$$

where I_{ph} points to the ideal source current generated via the solar light on the PV cell. This ideal source current is fully dependent on the solar irradiance, the current I_D that is flowing through the diode D, and the shunt current I_{sh} that flows through the shunt resistance R_p.

The current through the diode and shunt resistor is given by [41]

$$I_D = I_0 \left[\left(\frac{V_{pv} + R_s I}{\alpha k T/q} \right) - 1 \right] \tag{2}$$

and

$$I_{sh} = \left(\frac{V_{pv} + R_s I}{R_p} \right) \tag{3}$$

where R_s is the small series resistance, k is the Boltzmann constant $(1.38 \times 10^{-23}$ K/J), I_0 is the leakage current of diode D at a given temperature T, V_{pv} represents the PV array output voltage, and α is the diode ideality factor, while q is the electron charge $(1.6 \times 10^{-19}$ C).

A practical PV array is the combination of parallel and series-connected PV cells. Note that PV cells, which are connected in parallel, enhance the output PV current, while a series connection of PV cells enhances PV output voltage. The output PV current I_{pv} of practical PV array is followed by [41]

$$I_{pv} = N_p I_{ph} - N_p I_0 \left[\left(\frac{V_{pv} + R_s I}{\alpha N_s k T/q} \right) - 1 \right] - \left(\frac{V_{pv} + R_s I}{R_p} \right) \tag{4}$$

where N_p and N_s are the number of PV cells connected in series and parallel. The relevant characteristic curve of a PV array, i.e., (PV) and (IV), are shown in Figures 2 and 3, subject to varying environmental conditions [42].

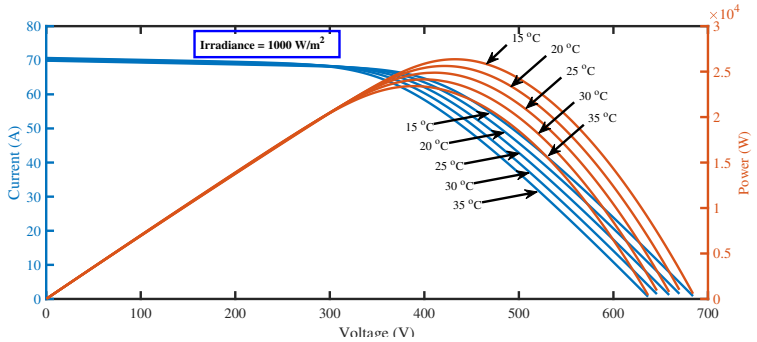

Figure 2. IV and PV characteristics curves of the PV array under varying temperature and constant irradiance.

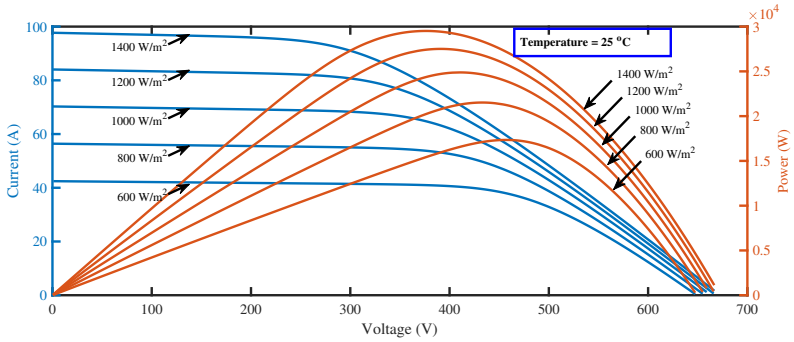

Figure 3. IV and PV characteristics curves of the PV array under fixed temperature and varying irradiance.

3. Non-Inverting DC-DC Buck-Boost Converter Modeling

This section presents brief modeling of the buck-boost converter. A complete circuit diagram of the PV panel connected to a non-inverting DC-DC BBC along with a core variable load is shown in Figure 4 (block A). From the diagram, it is clear that V_{pv} is considered as source voltage, which is obtained from the PV panel, while two semiconductor switches, S_1 and S_2, are used for the control purpose. Besides these, it also consists of two diodes D_1 and D_2, an inductor L, an input capacitor C_i, an output capacitor C_0, and a variable load, which are further composed of a charging station E_b and a variable resistive load R_L . Additionally, note that switch S_3 is connected between resistive and charging station load.

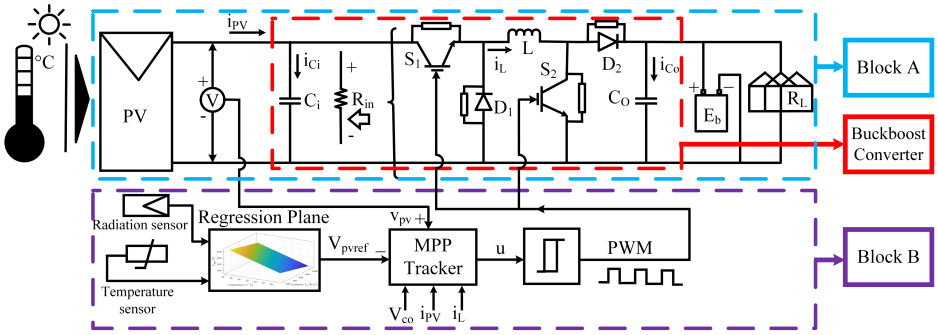

Figure 4. Complete model of PV system.

Before going into the modeling, some assumptions are made. It is assumed that both the switches and diodes are ideal, i.e., both observe zero losses. In addition, for the sake of simplicity, the resistances of the inductor and capacitors are assumed to be zero. It is also important to assume that the converter operates in the continuous conduction mode (C.C.M.).

It is worth noting that the converter operates in two distinct modes. In mode 1, both switches S_1 and S_2 are considered OFF, while both the diodes D_1 and D_2 are considered ON. Similarly, in mode 2, both switches S_1 and S_2 are considered ON, while both diodes D_1 and D_2 are considered OFF.

The dynamical equations of the BBC in mode 1 (accompanied by charging station E_b and variable resistive load R_L) can be obtained by applying Kirchoff's law of voltage as follows

$$\begin{bmatrix} \frac{dv_{pv}}{dt} \\ \frac{di_L}{dt} \\ \frac{dv_0}{dt} \end{bmatrix} = \begin{bmatrix} 0 & -\frac{1}{C_i} & 0 \\ \frac{1}{L} & 0 & 0 \\ 0 & 0 & -\frac{1}{R_b C_0} - \frac{1}{RC_0} \end{bmatrix} \begin{bmatrix} v_{pv} \\ i_L \\ v_0 \end{bmatrix} + \begin{bmatrix} \frac{I_{pv}}{C_i} \\ 0 \\ \frac{E_b}{R_b C_0} \end{bmatrix} \tag{5}$$

Similarly, in mode 2, the dynamical equation appears as follows.

$$\begin{bmatrix} \frac{dv_{pv}}{dt} \\ \frac{di_L}{dt} \\ \frac{dv_0}{dt} \end{bmatrix} = \begin{bmatrix} 0 & 0 & 0 \\ 0 & 0 & \frac{-1}{L} \\ 0 & \frac{1}{C_0} & -\frac{1}{R_bC_0} - \frac{1}{RC_0} \end{bmatrix} \begin{bmatrix} v_{pv} \\ i_L \\ v_0 \end{bmatrix} + \begin{bmatrix} \frac{i_{pv}}{C_i} \\ 0 \\ \frac{E_b}{R_bC_0} \end{bmatrix} \tag{6}$$

Based on the capacitor charge balance and inductor volt-second balance principles, the average dynamic model of the entire system depicted in Figure 4 (block A) is represented as follows:

$$\begin{bmatrix} \frac{d\bar{v}_{pv}}{dt} \\ \frac{d\bar{i}_L}{dt} \\ \frac{d\bar{v}_0}{dt} \end{bmatrix} = \begin{bmatrix} 0 & -\frac{D}{C_i} & 0 \\ \frac{D}{L} & 0 & \frac{D-1}{L} \\ 0 & \frac{1-D}{C_0} & -\frac{1}{R_bC_0} - \frac{1}{RC_0} \end{bmatrix} \begin{bmatrix} \bar{v}_{pv} \\ \bar{i}_L \\ \bar{v}_0 \end{bmatrix} + \begin{bmatrix} \frac{i_{pv}}{C_i} \\ 0 \\ \frac{E_b}{R_bC_0} \end{bmatrix} \tag{7}$$

where D is the duty cycle and $\bar{v}_{pv}$, $\bar{i}_L$, and $\bar{v}_0$ represent the average values of v_{pv}, i_L, and v_0, respectively.

The voltage conversion ratio of the non-inverted DC-DC BBC can be represented in the following form [42].

$$\frac{v_o}{v_{pv}} = \frac{D}{1-D} \tag{8}$$

In the case of ideal power transfer (subject to assumption 1), the input power equals to the output power, $P_i = P_0$. The relationship of the input impedance R_{in} and output impedance R_0 can be expressed in the following equation [42].

$$R_{in} = \left(\frac{1-D}{D}\right)^2 R_0 \tag{9}$$

It is worth mentioning that, apart from the variable resistive load and charging station, the system may experience some input channel uncertainties (caused by the malfunction or states coupling effects). Consequently, the average dynamic model (7) in new variables (i.e., by renaming v_{pv}, i_L, v_0, v_{pvref}, and D as x_1, x_2, x_3, x_{1ref}, and u, respectively) is written as follows:

$$\dot{x}_1 = \frac{i_{pv}}{C_i} - \frac{x_2}{C_i}(u + F(x,t)) \tag{10}$$

$$\dot{x}_2 = -\frac{x_3}{L} + \frac{(x_1 + x_3)}{L}u \tag{11}$$

$$\dot{x}_3 = (E_b - x_3)\frac{1}{R_bC_0} - \frac{x_3}{RC_0} - \frac{x_2}{C_0}(1-u) \tag{12}$$

where i_{pv} is the PV current, x=$[x_1, x_2, x_3]^T \epsilon R^3$ is the state vector and $F(x,t)$ represents the uncertainties about which the following assumption is made.

Assumption 1. *Assume that the uncertain term can be subdivided into structured and unstructured terms i.e.*

$$F(x,t) = \vartheta_s(x) + \vartheta_u(x,t) \tag{13}$$

Assumption 2. *The uncertain components are also assumed bounded i.e.*

$$\vartheta_s(x) = \delta\Psi(x) \tag{14}$$

and

$$|\vartheta_u(x,t)| \leqslant \Omega \tag{15}$$

where Ω is a positive constant.

Remark 1. *The partially known structured uncertainty in* (14) *is expressed as a product of a known base function* $\Psi(x)$ *and an uncertain constant parameter* δ. δ *can be any parametric change that occurs in the PV system's internal parameters. The estimate of this parameter will be designed later.*

The system (10)–(12) is the final model which will be used in the subsequent sections.

4. Proposed Uncertainty Tolerant MPPT Control Design

In this work, the core objective is that the output voltage v_{pv} of a non-inverted BBC should track a reference voltage v_{pvref}. The v_{pvref} is defined in such a way that at each point of it one may obtain the maximum power. So, the maximum power can be extracted from the existing system by tracking the reference voltage. This job of reference tracking can be achieved by continuously changing the converter duty cycle D through an output feedback controller (one may say it M.P.P. tracker) shown in Figure 4 (Block B).

The proposed control law will need the values of x_{1ref}, which will be estimated via neuro-fuzzy algorithm under varying temperature and irradiance. In addition, the controller is also using the inductor current x_2 as known data, which is generally not available in a practical scenario. Therefore, an appropriate velocity observer and the flatness property will be proposed. In the later part, we will focus on the certainty equivalence-based control strategies. So we proceed further by designing the reference voltage generation, velocity observer design, and certainty equivalence techniques.

4.1. Neuro-Fuzzy Algorithm Based Reference Voltage Generation

The proposed research work's neuro-fuzzy network (N.F.N.) is based on Takagi-Sugeno fuzzy inference system. We have adapted the reference voltage generated in [42]. The N.F.N. consists of varying irradiance and temperature as inputs. The input layer is followed by a fuzzification layer based on the Gaussian membership function for each individual variable. In the third step, the "IF-THEN" fuzzy rule is adopted. The output of this layer is fed into the normalization layer, which is further followed by an output layer. The output layer gives the estimated reference voltage v_{pvref}, expressed as x_{1ref}. The N.F.N. is shown in Figure 5, while the relevant estimated x_{ref} against varying temperature and irradiance is shown in Figure 6.

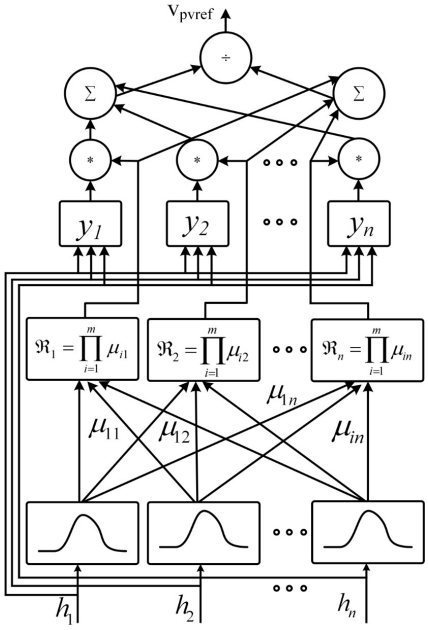

Figure 5. Neuro-fuzzy architecture.

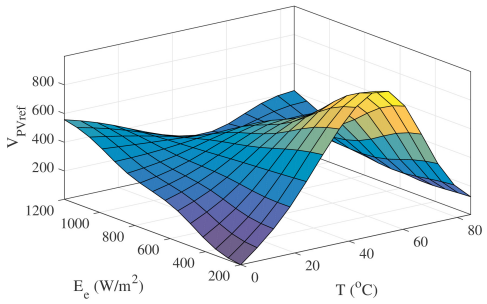

Figure 6. 3–D plane for v_{pvref} vs. E_e(W/m^2) and T(°C).

4.2. A Velocity Observer

To portray a practical scenario of the presented problem, i.e., to make the PV system sensorless, the proposed controller will need x_2, the estimated reference, and its higher derivatives. Therefore, a suitable velocity observer, which converges in finite time to the actual value, is presented here. Assume that the PV output x_1 is available and x_{1ref} is also available (via NFL). To estimate the derivative of the PV-output voltage, an auxiliary system of the following form is developed:

$$\dot{\bar{x}}_1 = \bar{x}_1 \tag{16}$$

$$\bar{x}_2 = \bar{\Delta}(x_1, x_2, x_3, t) \tag{17}$$

This system has two outputs, i.e., $\bar{x}_1$ and $\bar{x}_2$, where $\bar{x}_1 = x_1$ and $\bar{x}_2 = \dot{x}_1$ (this remains true for PV system). The term $\Delta(x_1, x_2, x_3, t)$ represents a bounded disturbance. Now, our aim is to estimate $\bar{x}_{2(e)}$, which in actual sense is the derivative of $\dot{x}_1$. The observer is proposed in the following form:

$$\dot{y}_1(t) = y_2 + \Lambda_1(t) \tag{18}$$

$$\dot{y}_2(t) = \Lambda_2(t) + \Delta\ (t) \tag{19}$$

where the variable y_1 represents the estimate of $\bar{x}_1$, y_2 is the estimated derivative of the $\bar{x}_2$, and $\Lambda_1(t)$ and $\Lambda_2(t)$ are the injection terms, defined as follows:

$$\Lambda_1(t) = \Big(\frac{k_1}{||x_1(t) - y_1(t)||^{\frac{1}{2}}} + k_2\Big)\big(x_1(t) - y_1(t)\big) \tag{20}$$

$$\Lambda_2(t) = \Big(\frac{k_3}{||x_1(t) - y_1(t)||} + k_4\Big)\big(x_1(t) - y_1(t)\big) \tag{21}$$

where k_i (i= 1,...,4) are positive constants, chosen according to the forthcoming inequalities. The error dynamics between (16), (17) and (18), (19), by defining $\sigma_1 = \bar{x}_1 - y_1$ and $\sigma_2 = \bar{x}_2 - y_2$, become

$$\dot{\sigma}_1 = \sigma_2 - \Big(\frac{k_1}{||\sigma_1||^{\frac{1}{2}}} + k_2\Big)\sigma_1 \tag{22}$$

$$\dot{\sigma}_2 = -\Big(\frac{k_3}{||\sigma_1||} + k_1\Big)\sigma_1 + \Delta\ (x_1, x_2, x_3, t) \tag{23}$$

The injection terms work like a supertwisting controller, and forces $\sigma_1 = \sigma_2 = 0$. Having met $\sigma_1 = 0$ and $\sigma_2 = 0$, we get $\bar{x}_2 = y_2$ for all $t \geqslant t_b$, where t_b is some time instant. It is reported in [43] that $(\sigma_1 = \sigma_2 = 0)$ is achieved only if one chooses the gains as follows:

$$k_1 > \sqrt{(2\delta_1)},\ \ k_4 > \frac{(\frac{3}{2}k_1^2k_2 + 3\delta_1k_2)^2}{k_3k_1^2 - 2\delta_1^2 - 3\delta_1k_1^2} + 2k_2^2 \tag{24}$$

$$k_2 > 0, \;\; k_3 > max(3\delta_1 + \frac{2\delta_1^2}{k_1^2}, -2k_1^2 + \delta_1) \tag{25}$$

The constraints (24) and (25) are fulfilled for sufficiently large k_i $(i = 1, 2, 3, 4)$ with respect to λ_1, where $\lambda_1 \geqslant || \triangle ||$.

Note that the convergence of this observer is independent of the controller convergence, i.e., the separation principle remains true here.

4.3. Certainty-Equivalence-Based Robust Sliding Mode Control (CERSMC)

The control task is that the actual PV voltage x_1 should follow an N.F.N.-based generated reference that provides maximum instantaneous power. To pursue this, an error is defined as follows:

$$\sigma = x_1 - x_{1ref(e)} \tag{26}$$

The Equation (26) is considered as a sliding surface for this strategy. The time derivative of (26) becomes

$$\dot{\sigma} = \frac{\partial}{\partial x1}\sigma(\dot{x}_1 - \dot{x}_{1ref(e)}) \tag{27}$$

Now, (27) along (10) becomes

$$\dot{\sigma} = \frac{i_{pv}}{C_i} - \frac{x_2}{C_i}\big(u + F(x,t)\big) - \dot{x}_{1ref(e)} \tag{28}$$

A fixed reference voltage (with different steps) is considered in the present study. Therefore, its time derivative $\dot{x}_{1ref(e)}$ becomes zero. So, it will appear in the following calculations. Before moving to the next step, it is suitable to define flatness property.

Definition 1. *The system is named as a flat system if any of its inputs/states/parameters are expressed as a function of flat outputs and their derivatives up to a finite order, for example:*

$$x_j = \Phi(x_i, \dot{x}_i, ..., x_k, \dot{x}_k, ..., u, \dot{u}, ...u_r) \tag{29}$$

where $x_i, \dot{x}_i, x_k, \dot{x}_k, u, \dot{u}, u_r$ are the states and the derivatives of the system's variables. For more details, the reader may see [44,45].

In this strategy, the control input is considered as sum of two components u_{eq} and u_d, where u_{eq} represents the equivalent part, whereas u_d is a discontinuous function. So,

$$u = u_{eq} + u_d \tag{30}$$

The control input u_{eq} governs the system trajectories when the constraint $\sigma = 0$ is met. This is designed by posing $\dot{\sigma} = 0$ (reported in (28)), and calculating for u while ignoring $F(x,t)$, one may get

$$u_{eq} = \frac{i_{pv}}{x_2} \tag{31}$$

In practice, the measurements of x_2 may not be available; therefore, using the velocity observer and Definition (1), one may obtain the estimated value of $x_{2(e)}$ as follows:

$$x_{2(e)} = \frac{C_i}{u}\left(\frac{i_{pv}}{Ci} - \dot{x}_{1(e)}\right) \tag{32}$$

where $\dot{x}_{1(e)}$ is the estimated velocity of x_1(via the velocity observer). Note that, in the present process, the value of the input u never becomes zero. Hence, the authors of (32) did not obatin singular results . Invoking (32) in (31), u_{eq} becomes

$$u_{eq} = i_{pv}\frac{C_i}{u}\left(\frac{i_{pv}}{C_i} - \dot{x}_{1(e)}\right) \tag{33}$$

which is a known quantity.

The expression of (28) along (31) takes the form

$$\dot{\sigma} = \delta a_1(x_1, x_2) + a_2(x_1, x_2, t) + u_d \tag{34}$$

where

$$-\Psi(x)\frac{\partial \sigma}{\partial x_1}.\left(\frac{x_2}{C_i}\right) = a_1(x_1, x_2) \tag{35}$$

$$-\frac{\partial \sigma}{\partial x_1}.\left(\frac{x_2}{C_i}\right)\vartheta_u(x, t) = a_2(x_1, x_2) \tag{36}$$

Now, the expression of u_d is chosen as follows:

$$u_d = -k_1\sigma - k_2 sign(\sigma) - \hat{\delta}a_1(x_1, x_2, t) \tag{37}$$

where k_1 and k_2 are controller gains which are chosen positive. The term $\hat{\delta}$ represents the estimated value of unknown parameter δ, which is chosen as follows:

$$\dot{\hat{\delta}} = \gamma\sigma a_1(x_1, x_2) \tag{38}$$

This choice of $\hat{\delta}$ will be elaborated in the following theorem.

Theorem 1. *If the following hold:*

i. Assumption 3 remains true;
ii. the sliding surface is chosen as (26);
iii. the equivalent control law u_{eq} as (31) (with detailed expression as (33));
iv. the discontinuous control component as (37);
v. the estimate of the unknown term (38) is fulfilled; and
vi. $k_2 > \Omega$. Then, sliding mode occurs along (26) and the system's output tracks the desired reference.

Proof. Consider a Lyapunov candidate function as follows:

$$V = \frac{1}{2}\sigma^2 + \frac{1}{2\gamma}\tilde{\delta}^2 \tag{39}$$

where γ is positive constant and $\hat{\delta}$-δ=$\tilde{\delta}$.

Considering the time derivative of the Lyapunov function

$$\dot{V} = \sigma\dot{\sigma} + \frac{1}{\gamma}\tilde{\delta}\dot{\hat{\delta}} \tag{40}$$

along (33), (34), and Assumption 3, one has

$$\dot{V} = \sigma\left(u_d + \delta a_1(x_1, x_2) + a_2(x_1, x_2, t)\right) - \frac{1}{\gamma}\tilde{\delta}\dot{\hat{\delta}} \tag{41}$$

Now, using (37), the above expression reduces to

$$\dot{V} = \sigma\left(-\bar{k}_1\sigma - \bar{k}_2 sign(\sigma) - a_1(x_1, x_2)\hat{\delta} + a_1(x_1, x_2)\delta + a_2(x_1, x_2, t)\right) - \frac{1}{\gamma}\tilde{\delta}\dot{\hat{\delta}}$$

$$\dot{V} = \sigma\left(-\bar{k}_1\sigma - \bar{k}_2 sign(\sigma) + a_1(x_1, x_2)(\delta - \hat{\delta}) + a_2(x_1, x_2, t)\right) - \frac{1}{\gamma}\tilde{\delta}\dot{\hat{\delta}}$$

$$\dot{V} = \sigma\left(-\bar{k}_1\sigma - \bar{k}_2 sign(\sigma) + a_2(x_1, x_2, t)\right) + a_1(x_1, x_2)\tilde{\delta}\sigma - \frac{1}{\gamma}\tilde{\delta}\dot{\hat{\delta}} \tag{42}$$

$$\dot{V} \leq -\bar{k}_1\sigma^2 - \bar{k}_2|\sigma| + |a_2(x_1, x_2, t)||\sigma| + \tilde{\delta}\left(a_1(x_1, x_2)\sigma - \frac{1}{\gamma}\dot{\hat{\delta}}\right)$$

$$\dot{V} \leq -\bar{k}_1\sigma^2 - |\sigma|\left(\bar{k}_2 - |a_2(x_1, x_2)|\right) + \tilde{\delta}\left(a_1(x_1, x_2)\sigma - \frac{1}{\gamma}\dot{\hat{\delta}}\right)$$

Now, by choosing $\bar{k}_2 \geqslant \eta + \Omega$ and $\dot{\hat{\delta}} = \gamma\sigma a_1(x_1, x_2)$, one gets the following:

$$\dot{V} \leqslant -\bar{k}_1\sigma^2 - \eta|\sigma| \tag{43}$$

where η and Ω are small positive constants. The authors of (43) show that sliding mode takes place across $\sigma = 0$. The detailed expression of the estimates of the unknown constant appears as follows:

$$\dot{\hat{\delta}} = \gamma\sigma\Psi(x)\frac{\partial}{\partial x_1}.\left(\frac{x_2}{Ci}\right) \tag{44}$$

This also shows that an equivalent value of the structured uncertainty is considered as a part of the control input, while the effects of the unstructured are nullified (suppressed) to a tolerable band. This completes the proof. □

4.4. Certainty-Equivalence-Based Robust Integral Sliding Mode Control (CERISMC)

The CERISMC performs very well; however, it remains sensitive to disturbances in the reaching phase. To confirm robustness for time t_0, a certainty equivalence-based ISMC is defined here. In this approach, the tracking error (26) is considered, and the integral sliding surface is defined as follows:

$$\bar{\sigma} = \sigma + \int_0^t \sigma d\tau \tag{45}$$

where the integral term helps in the elimination of the reaching phase and chattering reduction. The time derivative of (45) along (10) becomes

$$\dot{\bar{\sigma}} = \frac{\partial\sigma}{\partial x_1}.(\dot{x}_1) - \frac{\partial\sigma}{\partial x_{1ref}}.(\dot{x}_{1ref}) + \sigma \tag{46}$$

Note that the value of the integrand in (46) should be chosen in such a way that $\sigma(0) + \int_0^{t_0}\sigma d\tau = 0$, where t_0 is the initial time.

$$\dot{\bar{\sigma}} = \frac{\partial\sigma}{\partial x_1}.\left(\frac{i_{pv}}{C_i} - \frac{x_2}{C_i}\left(F(x,t) + u\right)\right) - \frac{\partial\sigma}{\partial x_{1ref}}.(\dot{x}_{1ref}) + \sigma \tag{47}$$

Now, considering the uncertain terms $F(x,t) = 0$ in (47) and posing $\dot{\bar{\sigma}} = 0$ and calculating for u_{eq}, one gets

$$u_{eq} = \frac{1}{\frac{\partial\sigma}{\partial x_1}.\left(\frac{x_2}{C_i}\right)}\left[\frac{\partial\sigma}{\partial x_1}.\left(\frac{i_{pv}}{C_i}\right)\right] - \frac{\partial\sigma}{\partial x_{1ref}}.(\dot{x}_{1ref}) \tag{48}$$

The control input, considered here, is defined as an algebraic sum of three components, i.e.,

$$u = u_0 + u_{eq} + u_d \tag{49}$$

where u_{eq} is constructed (48). Now, we will pursue for the other two components. An alternate expression of (47) is given as follows:

$$\dot{\bar{\sigma}} = \frac{\partial \sigma}{\partial x_1}.\left(\frac{i_{pv}}{C_i}\right) + \frac{\partial \sigma}{\partial x_1}.\left(-\frac{x_2}{C_i}\right)\Big(F(x,t) + u_0 + u_{eq} + u_d\Big) \tag{50}$$

Now, keeping in view Assumption 3, one has

$$\dot{\bar{\sigma}} = \frac{\partial \sigma}{\partial x_1}.\left(\frac{i_{pv}}{C_i}\right) + \frac{\partial \sigma}{\partial x_1}.\left(-\frac{x_2}{C_i}\right)\Big(\vartheta_s(x) + \vartheta_u(x,t) + u_0 + u_{eq} + u_d\Big) \tag{51}$$

To cancel the effects of the structured uncertainties, an equivalent cancellation law u_0 is proposed as follows:

$$u_0 = -\delta\Psi(x) \tag{52}$$

where δ represents the estimated value of the unknown parameter. Its details will be reported in the stability analysis.

In this work, the discontinuous control component, u_d, is defined to be

$$u_d = \frac{1}{\frac{\partial \sigma}{\partial x_1}.\left(\frac{x_2}{C_i}\right)}\Big(k_1\sigma - k_2 sign(\bar{\sigma})\Big) \tag{53}$$

where k_1 and k_2 are the controller gains, whose choice will be given in the stability study. The overall control law (54) will appear as follows:

$$u = -\delta\Psi(x) + \frac{1}{\frac{\partial \sigma}{\partial x_1}.\left(\frac{x_2}{C_i}\right)}\left[\frac{\partial \sigma}{\partial x_1}.\left(\frac{i_{pv}}{C_i}\right)\right] - \frac{\partial \sigma}{\partial x_{1ref}}.(\dot{x}_{1ref}) + \frac{1}{\frac{\partial \sigma}{\partial x_1}.\left(\frac{x_2}{C_i}\right)}\Big(k_1\sigma - k_2 sign(\bar{\sigma})\Big) \tag{54}$$

This control law will enforce sliding mode along the sliding surface given in (45). The following theorem (very similar to Theorem 1) is stated.

Theorem 2. *If the following hold:*

i. Assumption 3 remains true;
ii. the sliding surface is chosen as (45);
iii. the equivalent control law u_{eq} as (48);
iv. the discontinuous control component as (53);
v. the estimate of unknown term (38) is fulfilled; and
vi. $k_1 > \Omega$. Then, sliding mode occur along (45) and the system's output tracks the desired reference.

Proof. The proof of this theorem is very similar to Theorem 1. The sliding manifolds (45), u_{eq} (48), and u_d (53) are changed from Theorem 1 with some additional terms. Therefore, their details are avoided here. □

Remark 2. *The adaptation law (38) may result in an accurate estimate of the structured uncertainty and it does not demand any constraint on the structured uncertainties.*

Remark 3. *If the uncertainty can be subdivided into structured and unstructured parts, then the controller gains can be reduced significantly. Consequently, this will also result in suppressed chattering.*

4.5. Stability of the Zero Dynamics

In the presented control design strategies, the sliding surfaces have a relative degree of one. Therefore, two differential equations remain, which claim to describe the internal dynamics. Their dynamics are given as follows:

$$\dot{x}_2 = -\frac{x_3}{L} + \frac{x_1 + x_2}{L}u \tag{55}$$

$$\dot{x}_3 = -\frac{x_2}{C_0} - \frac{R + R_b}{RR_b}x_3 + \frac{1}{R_bC_0}E_b + \frac{x_2}{C_0}u \tag{56}$$

Since the system's output x_1 is driven by the control input u, to calculate the zero dynamic, we assume $x_1 = 0$ and $u = 0$ in the above internal dynamics. Thus, one comes up with this

$$\begin{bmatrix} \dot{x}_2 \\ \dot{x}_3 \end{bmatrix} = \begin{bmatrix} 0 & -\frac{1}{L} \\ -\frac{1}{C_0} & -\frac{R+R_b}{RR_bC_0} \end{bmatrix} \begin{bmatrix} x_2 \\ x_3 \end{bmatrix} + \begin{bmatrix} 0 \\ \frac{E_b}{R_bC_0} \end{bmatrix} \tag{57}$$

It is a non-homogeneous linear time-invariant system. This system has all the poles in the left half-plane, which confirms the convergence of x_2 and x_3 to the vicinity of the origin, i.e., these states ensure practical asymptotic convergence to the origin.

5. Results and Discussion

The newly proposed control laws are applied to the PV system presented in the modeling section. All the initial conditions of the system's states are chosen zero. The typical parameters of the PV array, converter, charging station, and variable load are given in Table 1, which are adapted from [42]. The simulations are carried out in MATLAB Simulink environment with a numerical solver (Ode23t(mod.stiff/Tranpezoidal)) method and variable-step. The environmental variation considered in this simulation is shown in Figure 7, while the load variation is shown in Figure 8. In addition, the structured and unstructured uncertainties introduced in the system carry the following expression:

$$F(x,t) = \begin{cases} 0.5sin(x_1) + 0.03sin(x_1)cos(5t) \\ for \quad 0.12 \leq t \leq 0.16 \end{cases} \tag{58}$$

In the simulation study, the comparison of CERSMC and CERISMC is made with the conventional ISMC and STA results. The attributes considered are reference tracking (in the presence of varying environmental variations; load variations; uncertainties of a structured and unstructured kind); maximum power extraction; efficiency; and performance indices such as integral absolute error, integral square error, integral time absolute error, and integral time square error.

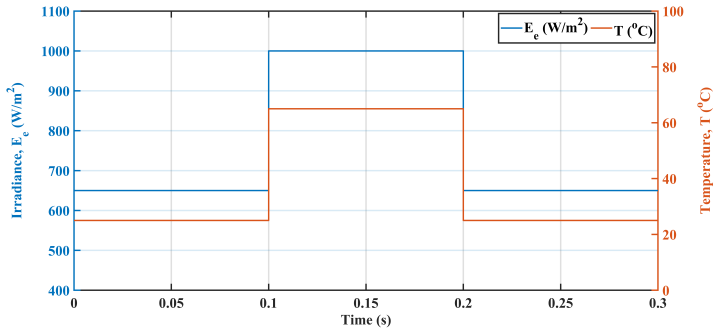

Figure 7. Variable E_e and Variable T profiles w.r.t time.

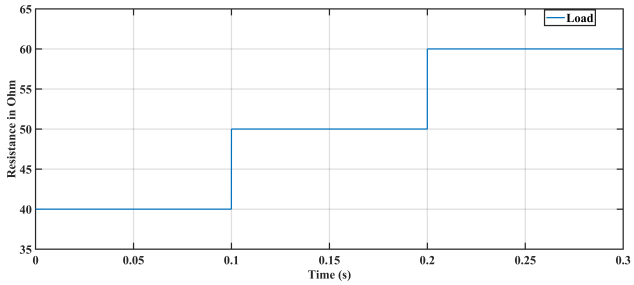

Figure 8. Variable resistive load.

Table 1. Parameters of the PV system.

Parameter	Unit	Value
Maximum power, P_{max}	W	1555
No. of PV cells per module, N_s		72
Open circuit voltage,V_{0c}	V	165.80
Short circuit current, I_{sc}	A	17.56
Voltage at MPP,V_{MPP}	V	102.60
Current at MPP, I_{MPP}	A	15.16
Inductor, L	mH	20
Input capacitor, C_{in}	mF	1
Output capacitor, C_{out}	uF	48
IGBT switching frequency, f_s	K_{Hz}	5
Charging battery, E_b	V	24
Internal resistance, R	Ω	0.65

The desired reference tracking of the PV-system for all the control strategies named above is shown in Figure 9. It is evident from the figure that the conventional STA and ISMC are slower in the rise time than those of CERSMC and CERISMC. This is one benefit of the proposed strategies. In the simulation, as we introduced the structured and unstructured uncertainties (according to Equation (58)), the conventional STA and ISMC lost the reference tracking, while our proposed CERSMC and CERISMC performed very well reference tracking. This is the second advantage of the currently proposed strategies. This attribute of reference tracking is demanding in practical applications. In the subfigure of Figure 9, it is clear that, at the instant of uncertainties, the proposed controllers are performing better in terms of tracking error, whereas the comparative controllers are de-tracking the desired reference, and, as a result, a considerable tracking error is formed.

Having looked at the power graphs in Figure 10, it is evident that the proposed strategies CERSMC and CERISMC resulted in fast maximum power extraction while both the conventional approaches ISMC and STA resulted in slower power extraction. It is also essential to note that the traditional strategies resulted in very poor power extraction because we introduced the uncertainties. This once again shows the robust nature of our newly proposed methods. Along with that, from the figure, it is clear that the phenomenon of chattering is more pronounced in STA and ISMC than our proposed controllers, which is once again due to the outstanding performance of proposed controllers. The converter successfully transfers the maximum power, to the charging station and variable load, with efficiencies greater than 98% in the case of CERSMC and CERISMC (see for details Figure 11), while STA and ISMC have low efficiencies. In a nutshell, the proposed strategies are far appealing in practical contexts for power systems' applications.

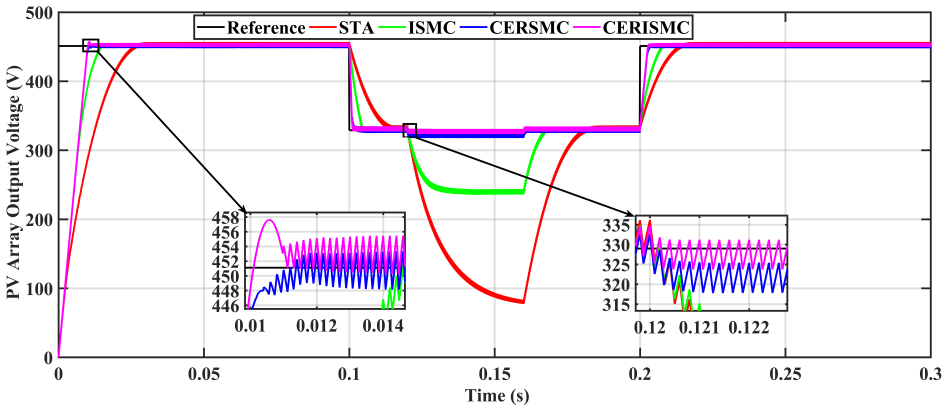

Figure 9. PV array output voltages under varying irradiance, temperature, load and a charging station.

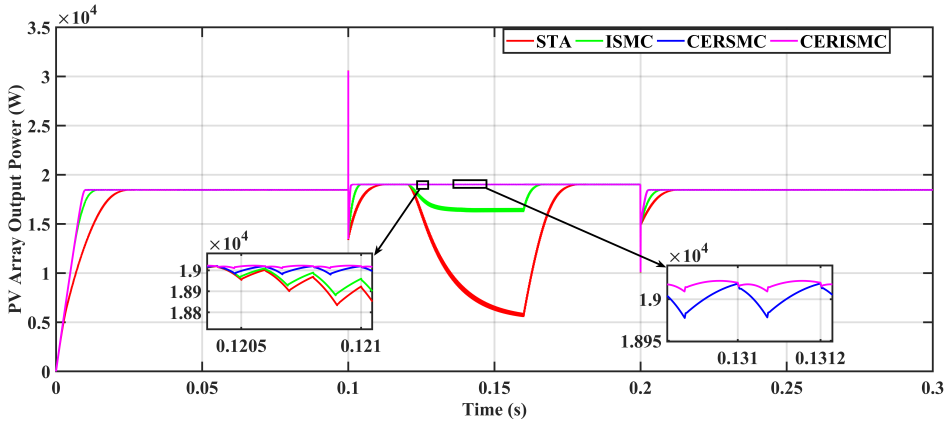

Figure 10. PV array output powers under varying irradiance, temperature, load and a charging station.

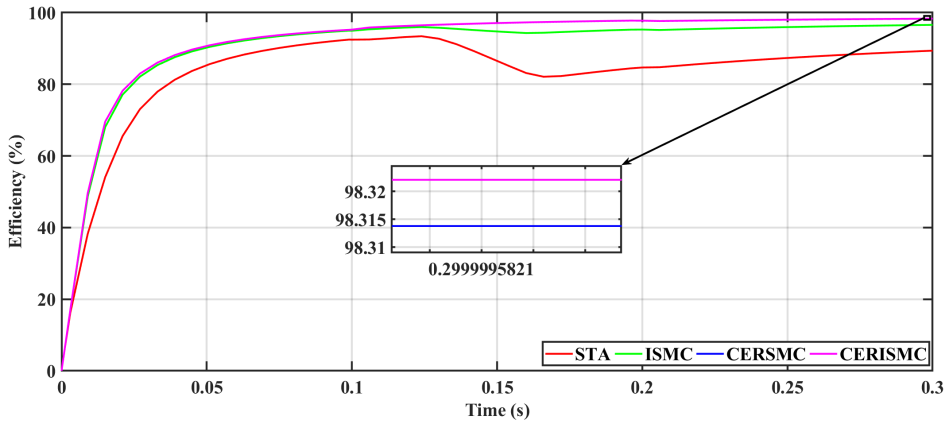

Figure 11. Efficiencies under varying irradiance, temperature, load and a charging station.

6. Conclusions

In this work, the main objective was to extract the maximum power from a PV array, which is accompanied by a BBC. To achieve this goal, first, the system was modeled under the action of varying temperature and irradiance. In addition, the system was also considered with a variable resistive load and charging station. Secondly, using a fuzzy neural network, a reference voltage was generated. By following the reference voltage, one may get the maximum power. So, our problem was reduced to voltage tracking controller design. Practically, only the PV voltage was considered to be available as known information. The remaining required states were recovered using a velocity observer and the flatness property of nonlinear systems. Having recovered the missing states, the CERSMC and CERISMC were proposed to track the NFN-based generated voltage. The stability of these controllers, in a closed-loop, was comprehensively presented in theorems. Finally, the claims were verified in the simulation results by comparing the proposed techniques with STA and ISMC. It was witnessed that the proposed control strategies are effective approaches to deal with such systems. The future work directions include adaptive control design against system parametric variations, practical implementation of the proposed controller on PV systems, an efficient inverter design to inject harmonics-free PV power to the grid, and its integration with the grid (as well as other energy sources such as fuel cell energy, biomass energy, and so on) .

Author Contributions: Conceptualization, Z.A. and Q.K.; methodology, Z.A., Q.K. and S.U.; software, Z.A., Q.K.; validation, Z.A. and S.U.; formal analysis, Z.A. and L.K.; investigation, S.A.M.K. and A.A.A.; writing—original draft preparation, Z.A. and Q.K.; writing—review and editing, Q.K., L.K., A.A.A. and S.U.; supervision, Q.K., L.K. and S.A.M.K.; project administration, Q.K. and S.U. All authors have read and agreed to the published version of the manuscript.

Funding: The APC was funded by A.A.A.

Data Availability Statement: Not applicable.

Conflicts of Interest: The authors declare no conflict of interest.

References

1. Zhao, Y.; Ball, R.; Mosesian, J.; De Palma, J.-F.; Lehman, B. Graph-Based Semi-supervised Learning for Fault Detection and Classification in Solar Photovoltaic Arrays. *IEEE Trans. Power Electron.* **2014**, *30*, 2848–2858. [CrossRef]
2. Motahhir, S.; Chouder, A.; El Hammoumi, A.; Benyoucef, A.S.; El Ghzizal, A.; Kichou, S.; Kara, K.; Sanjeevikumar, P.; Silvestre, S. Optimal Energy Harvesting From a Multistrings PV Generator Based on Artificial Bee Colony Algorithm. *IEEE Syst. J.* **2020**, *15*, 4137–4144. [CrossRef]
3. Chtita, S.; Derouich, A.; El Ghzizal, A.; Motahhir, S. An improved control strategy for charging solar batteries in off-grid photovoltaic systems. *Sol. Energy* **2021**, *220*, 927–941. [CrossRef]
4. Raheem, A.; Abbasi, S.A.; Memon, A.; Samo, S.R.; Taufiq-Yap, Y.H.; Danquah, M.K.; Harun, R. Renewable energy deployment to combat energy crisis in Pakistan. *Energy Sustain. Soc.* **2016**, *6*, 16. [CrossRef]
5. Kabir, E.; Kumar, P.; Kumar, S.; Adelodun, A.A.; Kim, K.H. Solar energy: Potential and future prospects. *Renew. Sustain. Energy Rev.* **2018**, *82*, 894–900. [CrossRef]
6. Arsalan, M.; Iftikhar, R.; Ahmad, I.; Hasan, A.; Sabahat, K.; Javeria, A. MPPT for photovoltaic system using nonlinear backstepping controller with integral action. *Sol. Energy* **2018**, *170*, 192–200. [CrossRef]
7. Haque, A. Maximum Power Point Tracking (MPPT) Scheme for Solar Photovoltaic System. *Energy Technol. Policy* **2014**, *1*, 115–122. [CrossRef]
8. Faifer, M.; Cristaldi, L.; Toscani, S.; Soulantiantork, P.; Rossi, M. Iterative model-based maximum power point tracker for photovoltaic panels. In Proceedings of the 2015 IEEE International Instrumentation and Measurement Technology Conference (I2MTC) Proceeding, Pisa, Italy, 11–14 May 2015; pp. 1273–1278.
9. Reisi, A.R.; Moradi, M.H.; Jamasb, S. Classification and comparison of maximum power point tracking techniques for photovoltaic system: A review. *Renew. Sustain. Energy Rev.* **2013**, *19*, 433–443. [CrossRef]
10. Poshtkouhi, S.; Varley, J.; Popuri, R.; Trescases, O. Analysis of distributed peak power tracking in photovoltaic systems. In Proceedings of the 2010 International Power Electronics Conference-ECCE Proceeding, Sapporo, Japan, 21–24 June 2010; pp. 942–947.
11. Poshtkouhi, S.; Palaniappan, V.; Fard, M.; Trescases, O. A general approach for quantifying the benefit of distributed power electronics for fine grained MPPT in photovoltaic applications using 3-D modeling. *IEEE Trans. Power Electron.* **2011**, *27*, 4656–4666. [CrossRef]
12. Punitha, K.; Devaraj, D.; Sakthivel, S. Artificial neural network based modified incremental conductance algorithm for maximum power point tracking in photovoltaic system under partial shading conditions. *Energy* **2013**, *62*, 330–340. [CrossRef]
13. Rezk, H.; Aly, M.; Al-Dhaifallah, M.; Shoyama, M. Design and hardware implementation of new adaptive fuzzy logic-based MPPT control method for photovoltaic applications. *IEEE Access* **2019**, *7*, 106427–106438. [CrossRef]
14. Nguyen, T.L.; Low, K.S. A global maximum power point tracking scheme employing DIRECT search algorithm for photovoltaic systems. *IEEE Trans. Ind. Electron.* **2010**, *57*, 3456–3467. [CrossRef]
15. Moshksar, E.; Ghanbari, T.; Samet, H.; Guay, M. Estimation-based extremum-seeking control: A real-time approach for improving energy efficiency in photovoltaic systems. *IEEE Syst. J.* **2018**, *13*, 3141–3152. [CrossRef]
16. Yang, B.; Zhong, L.; Zhang, X.; Shu, H.; Yu, T.; Li, H.; Sun, L. Novel bio-inspired memetic salp swarm algorithm and application to MPPT for PV systems considering partial shading condition. *J. Clean. Prod.* **2019**, *215*, 1203–1222. [CrossRef]
17. Titri, S.; Larbes, C.; Toumi, K.Y.; Benatchba, K. A new MPPT controller based on the Ant colony optimization algorithm for Photovoltaic systems under partial shading conditions. *Appl. Soft Comput.* **2017**, *58*, 465–479. [CrossRef]
18. Soufyane Benyoucef, A.; Chouder, A.; Kara, K.; Silvestre, S. Artificial bee colony based algorithm for maximum power point tracking (MPPT) for PV systems operating under partial shaded conditions. *Appl. Soft Comput.* **2015**, *32*, 38–48. [CrossRef]
19. Dhople, S.V.; Davoudi, A.; Dominguez-Garcia, A.D.; Chapman, P.L. A unified approach to reliability assessment of multiphase dc-dc converters in photovoltaic energy conversion systems. *IEEE Trans. Power Electron.* **2012**, *27*, 739–751. [CrossRef]
20. Yang, S.; Bryant, A.; Mawby, P.; Xiang, D.; Ran, L.; Tavner, P. An industry-based survey of reliability in power electronic converters. *IEEE Trans. Ind. Appl.* **2011**, *47*, 1441–1451. [CrossRef]
21. Neeb, C.; Boettcher, L.; Conrad, M.; De Doncker, R.W. Innovative and reliable power modules: A future trend and evolution of technologies. *IEEE Ind. Electron. Mag.* **2014**, *8*, 6–16.
22. Gonz´alez, M.; Raison, B.; Bacha, S.; Bun, L. Fault diagnosis in a grid-connected photovoltaic system by applying a signal approach. In Proceedings of the 37th Annual Conference of the IEEE Industrial Electronics Society (IECON), Melbourne, Australia, 7–10 November 2011; pp. 1354–1359.
23. Potamianos, P.G.; Mitronikas, E.D.; Safacas, A.N. Open-circuit fault diagnosis for matrix converter drives and remedial operation using carrier-based modulation methods. *IEEE Trans. Ind. Electron.* **2013**, *61*, 531–545.
24. Brunson, C.; Empringham, L.; Lillo, L.D.; Wheeler, P.; Clare, J. Open-Circuit Fault Detection and Diagnosis in Matrix Converters. *IEEE Trans. Power Electron.* **2015**, *30*, 2840–2847. [CrossRef]

25. Wu, R.; Blaabjerg, F.; Wang, H.; Liserre, M.; Iannuzzo, F. Catastrophic failure and fault-tolerant design of igbt power electronic converters-an overview. In Proceedings of the 39th Annual Conference of the IEEE Industrial Electronics Society IECON, Vienna, Austria, 10–13 November 2013; pp. 507–513.
26. Youssef, F.; Sbita, L. Sensors fault diagnosis and fault tolerant control for grid connected PV system. *Int. J. Hydrogen Energy* **2017**, *42*, 8962–8971. [CrossRef]
27. Houssein, A.; Heraud, N.; Souleiman, I.; Pellet, G. Monitoring and fault diagnosis of photovoltaic panels. In Proceedings of the 2010 IEEE International Energy Conference Proceeding, Manama, Bahrain, 18–22 December 2010; pp. 389–394.
28. Akram, M.N.; Lotfifard, S. Modeling and health monitoring of dc side of photovoltaic array. *IEEE Trans. Sustain. Energy* **2015**, *6*, 1245–1253. [CrossRef]
29. Jamshidpour, E.; Poure, P.; Saadate, S. Photovoltaic systems reliability improvement by real-time fpga-based switch failure diagnosis and fault tolerant dc–dc converter. *IEEE Trans. Ind. Electron.* **2015**, *62*, 7247–7255. [CrossRef]
30. Lin, X.; Wang, Y.; Pedram, M.; Kim, J.; Chang, N. Designing fault-tolerant photovoltaic systems. *IEEE Design Test* **2013**, *31*, 76–84. [CrossRef]
31. Khan, Q.; Akmeliawati, R. Neuro-adaptive dynamic integral sliding mode control design with output differentiation observer for uncertain higher order mimo nonlinear systems. *Neurocomputing* **2017**, *226*, 126–134. [CrossRef]
32. Ullah, S.; Khan, Q.; Mehmood, A.; Kirmani, S.A.M.; Mechali, O. Neuro-Adaptive Fast Integral Terminal Sliding Mode Control Design with Variable Gain Robust Exact Differentiator for Under-Actuated Quadcopter UAV. *ISA Trans.* **2022**, *120*, 293–304. [CrossRef]
33. Ullah, S.; Khan, Q.; Mehmood, A.; Akmeliawat, R. Integral backstepping integral sliding mode control of underactuated nonlinear electromechanical systems. *Control. Eng. Appl. Infor.* **2019**, *21*, 42–50.
34. Reichhartinger, M.; Horn, M. Cascaded sliding-mode control of permanent magnet synchronous motors. In Proceedings of the 12th International Workshop on Variable Structure Systems, Mumbai, India, 12–14 January 2012; pp. 173–177.
35. Boiko, I.; Fridman, L.; Pisano, A.; Usai, E. Analysis of chattering in sys- tems with second-order sliding modes. *IEEE Trans. Autom.* **2007**, *52*, 2085–2102. [CrossRef]
36. Barth, A.; Reichhartinger, M.; Reger, J.; Horn, M.; Wulff, K. Lyapunov- design for a super-twisting sliding-mode controller using the certainty- equivalence principle. *IFAC-PapersOnLine* **2015**, *48*, 860–865. [CrossRef]
37. Barth, A.; Reichhartinger, M.; Wulff, K.; Horn, M.; Reger, J. Certainty equivalence adaptation combined with super-twisting sliding-mode control. *Int. J. Control.* **2016**, *89*, 1767–1776. [CrossRef]
38. Sanchez, T.; Moreno, J.A. A constructive lyapunov function design method for a class of homogeneous systems. In Proceedings of the the 53rd IEEE Conference on Decision and Control, Los Angeles, CA, USA, 15–17 December 2014; pp. 5500–5505.
39. Moreno, J., Sanchez, T., Cruz-Zavala, E. (2014). Una función de lyapunov suave para el algoritmo super-twisting. In Proceedings of the Memorias del XVI Congreso Latinoamericano de Control Automático (CLCA), Quintana Roo, Mexico, 14–17 October 2014; pp. 182–187.
40. Gray, J.L. The physics of the solar cell. *Handb. Photovolt. Sci. Eng.* **2003**, *2*, 82–128.
41. Villalva, M.G.; Gazoli, J.R.; Filho, E.R. Comprehensive approach to modeling and simulation of photovoltaic arrays. *IEEE Trans. Power Electron.* **2009**, *24*, 1198–1208. [CrossRef]
42. Ali, K.; Khan, L.; Khan, Q.; Ullah, S.; Ahmad, S.; Mumtaz, S.; Karam, F.W. Robust integral backstepping based nonlinear mppt control for a pv system. *Energies* **2019**, *12*, 3180. [CrossRef]
43. Nagesh, I.; Edwards, C. A multivariable super-twisting sliding mode approach. *Automatica* **2014**, *50*, 984–988. [CrossRef]
44. Sira-Ramirez, H.; Agrawal, S.K. *Differentially Flat Systems*; CRC Press: Boca Raton, FL, USA, 2004.
45. Iqbal, M.; Bhatti, A.I.; Ayubi, S.I.; Khan, Q. Robust parameter estimation of nonlinear systems using sliding-mode differentiator observer. *IEEE Trans. Ind. Electron.* **2010**, *58*, 680–689. [CrossRef]